

Molecular Docking and Three-Dimensional Quantitative Structure–Activity Relationship Studies on the Binding Modes of Herbicidal 1-(Substituted Phenoxyacetoxy)alkylphosphonates to the E1 Component of Pyruvate Dehydrogenase

HAO PENG, TAO WANG,[†] PENG XIE, TING CHEN,[‡] HONG-WU HE,*
AND JIAN WAN*

Key Laboratory of Pesticide and Chemical Biology, Ministry of Education, and College of Chemistry,
Central China Normal University, Wuhan 430079, People's Republic of China

Molecular docking and three-dimensional quantitative structure–activity relationship (3D-QSAR) studies on the title compounds were performed to explore the possible inhibitory mechanism. To determine the probable binding conformations of the title phosphonate derivatives, the most potent compound **12** was chosen as a standard template and docked into the active site of PDHc E1. On the basis of the binding conformations, highly predictive 3D-QSAR models were developed with q^2 values of 0.872 and 0.873 for comparative molecular field analysis (CoMFA) and comparative molecular similarity indices analysis (CoMSIA), respectively. The predictive abilities of these models were validated by using a set of compounds that were not included in the training set. Both the CoMFA and the CoMSIA field distributions are in good agreement with the spatial and electronic structural characteristics of the binding groove of PDHc E1 selected in this work. Mapping the 3D-QSAR models to the active site of PDHc E1 provides new insight into the protein–inhibitor interaction mechanism, which is most likely valuable and applicable for designing highly active compounds in the future.

KEYWORDS: 1-(Substituted phenoxyacetoxy)alkylphosphonates; herbicidal activities; 3D-QSAR; molecular docking; binding model; pyruvate dehydrogenase complex

INTRODUCTION

Pyruvate dehydrogenase complex (PDHc) is already known to be a site of pesticide action, because it plays a pivotal role in cellular metabolism catalyzing the oxidative decarboxylation of pyruvate and the subsequent acetylation of coenzyme A (CoA) to acetyl-CoA (1–4). The complex consists of three enzymes and a number of cofactors. Pyruvate dehydrogenase E1 component (PDHc E1, E.C. 1.2.4.1) is the initial member of PDHc, which catalyzes the first step of the multistep process, using thiamine diphosphate (ThDP) and Mg^{2+} as cofactors (5–7), so PDHc E1 is of interest from the point of view of agrochemical design. An attempt to design inhibitors of PDHc E1 as herbicides using biochemical reasoning was reported by Baillie et al. (8). Series of acylphosphinates and acylphosphonates have been prepared as mechanism-based inhibitors of PDHc, because their lowest homologues are regarded as bioisosteres of pyruvate (acetyl formate) (9). Baillie et al. demonstrated that some

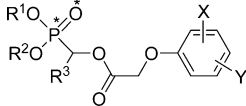
acetylphosphinates and acetylphosphonates showed modest herbicidal activity due to their inhibition against PDHc (8); however, the activity of them was not sufficiently high for full development as herbicides (8–10). We began a systematic, long-term study aiming to design new PDHc E1 inhibitors with phosphonate structure as potential herbicides. A series of 1-(substituted phenoxyacetoxy)alkylphosphonate derivatives (Table 1) were synthesized and shown to be endowed with notable herbicidal activities (11–15), and some of them have been demonstrated as inhibitors of PDHc E1 in our previous work (16–18). The ecological effects evaluation showed that some selected compounds are of low toxicity to bee, birds, silkworms, and fishes and are safe for the following crops.

It is very interesting that the herbicidal activities of title compounds are positively correlated with the inhibition of PDHc E1. Fortunately, the X-ray structure of PDHc E1-ThDP- Mg^{2+} and the analogues of PDHc E1-ThTDP (thiamine 2-thiothiazolone diphosphate)- Mg^{2+} have recently been determined and the active sites of two enzyme complexes have similar three-dimensional structures (19, 20). These crystal structure studies provided not only insights into the probable interaction mechanism of the PDHc E1 with the inhibitors but also valuable clues for the prediction of active sites. All thiamin-dependent

* To whom correspondence should be addressed. Tel/Fax: +86-27-67867960. E-mail: he1208@mail.ccnu.edu.cn or jianwan@mail.ccnu.edu.cn.

[†] Current address: College of Chemistry and Chemical Engineering, Jiangxi Normal University, Nanchang 330022, China.

[‡] Current address: Faculty of Material Science and Chemical Engineering, China University of Geosciences, Wuhan 430074, China.

Table 1. Structure and Biological Activities of Molecules Used in Training and Test Sets


compd	R ¹	R ²	R ³	X	Y	pIC ₅₀
1	CH ₃	CH ₃	2-furyl	3-F	H	4.17
2	CH ₃	CH ₃	2-furyl	4-F	H	5.74
3	CH ₃	CH ₃	2-furyl	4-Cl	H	6.19
4	CH ₃	CH ₃	2-furyl	2-Cl	4-Cl	6.47
5 ^a	CH ₃	CH ₃	2-furyl	2-Cl	6-Cl	3.49
6	CH ₃	CH ₃	2-furyl	2-Cl	3-Cl	3.35
7	CH ₃	CH ₃	2-furyl	2-CH ₃	4-Cl	5.42
8	CH ₃	CH ₃	2-furyl	3-CH ₃	4-Cl	5.44
9	CH ₃	CH ₃	2-furyl	2-Cl	5-CH ₃	4.06
10 ^a	CH ₃	CH ₃	2-thienyl	3-F	H	3.90
11	CH ₃	CH ₃	2-thienyl	4-F	H	5.58
12	CH ₃	CH ₃	2-thienyl	2-Cl	4-Cl	6.55
13	CH ₃	CH ₃	2-thienyl	4-Cl	H	6.24
14	CH ₃	CH ₃	2-thienyl	2-Cl	6-Cl	3.75
15 ^a	CH ₃	CH ₃	2-thienyl	2-Cl	3-Cl	3.23
16	CH ₃	CH ₃	2-thienyl	2-CH ₃	4-Cl	6.33
17	CH ₃	CH ₃	2-thienyl	3-CH ₃	4-Cl	5.63
18	CH ₃	CH ₃	2-thienyl	2-Cl	5-CH ₃	4.29
19	CH ₃	CH ₃	phenyl	3-F	H	3.95
20 ^a	CH ₃	CH ₃	phenyl	4-F	H	5.82
21	CH ₃	CH ₃	phenyl	4-Cl	H	6.37
22	CH ₃	CH ₃	phenyl	2-Cl	6-Cl	4.07
23	CH ₃	CH ₃	phenyl	2-Cl	3-Cl	3.64
24	CH ₃	CH ₃	phenyl	2-CH ₃	4-Cl	6.45
25 ^a	CH ₃	CH ₃	phenyl	3-CH ₃	4-Cl	5.59
26	CH ₃	CH ₃	phenyl	2-Cl	5-CH ₃	4.14
27	CH ₃	CH ₃	2-Cl Ph	3-CF ₃	H	5.10
28	CH ₃	CH ₃	4-Cl Ph	3-CF ₃	H	5.16
29	CH ₃	CH ₃	3-Cl Ph	3-CF ₃	H	4.84
30 ^a	CH ₃	CH ₃	3,4-2Cl Ph	3-CF ₃	H	5.08
31	CH ₃	CH ₃	4-CH ₃ Ph	3-CF ₃	H	5.13
32	CH ₃	sodium	2-furyl	2-Cl	4-Cl	6.35
33	CH ₃	sodium	2-pyridinyl	2-Cl	4-Cl	6.24
34	CH ₃	sodium	phenyl	2-Cl	4-Cl	6.02
35 ^a	CH ₃	sodium	2-Cl Ph	2-Cl	4-Cl	6.04
36	CH ₃	sodium	4-Cl Ph	2-Cl	4-Cl	5.88
37	CH ₃	sodium	2,4-2Cl Ph	2-Cl	4-Cl	5.99
38	CH ₃	sodium	3,4-2Cl Ph	2-Cl	4-Cl	6.05
39	CH ₃	sodium	4-CH ₃ O Ph	2-Cl	4-Cl	6.02
40 ^a	CH ₃	sodium	4-F Ph	2-Cl	4-Cl	6.11
41	CH ₃	sodium	3-NO ₂ Ph	2-Cl	4-Cl	5.91
42	CH ₃	sodium	4-CH ₃ Ph	2-Cl	4-Cl	5.87
43	CH ₃	CH ₃	CH ₃	3-F	H	3.95
44	CH ₃	CH ₃	CH ₃	4-F	H	5.82
45 ^a	CH ₃	CH ₃	CH ₃	4-Cl	H	6.37
46	CH ₃	CH ₃	CH ₃	2-Cl	6-Cl	4.00
47	CH ₃	CH ₃	CH ₃	2-Cl	3-Cl	3.68
48	CH ₃	CH ₃	CH ₃	2-CH ₃	4-Cl	6.36
49	CH ₃	CH ₃	CH ₃	3-CH ₃	4-Cl	5.53
50 ^a	CH ₃	CH ₃	CH ₃	2-Cl	5-CH ₃	4.31
51	CH ₃	CH ₃	CCl ₃	3-F	H	4.08
52	CH ₃	CH ₃	CCl ₃	4-F	H	5.93
53	CH ₃	CH ₃	CCl ₃	4-Cl	H	6.14
54	CH ₃	CH ₃	CCl ₃	2-Cl	6-Cl	3.94
55 ^a	CH ₃	CH ₃	CCl ₃	2-Cl	3-Cl	4.15
56	CH ₃	CH ₃	CCl ₃	2-CH ₃	4-Cl	6.40
57	CH ₃	CH ₃	CCl ₃	3-CH ₃	4-Cl	5.46
58	CH ₃	CH ₃	CCl ₃	2-Cl	5-CH ₃	4.12

^a The compounds in the test set for model validation.

reactions, in which the cofactor ThDP plays an important role, are initiated by the formation of a covalent adduct between the substrate and the cofactor through the C2 atom of the thiazolium ring (20). It is thus reasonable to assume that the active sites are located around the cofactor ThDP. However, there is so far

no report about the binding model of similar phosphonate derivatives with the receptor, which is crucial for the construction of agrophore (21) models and the design of potential inhibitors and novel herbicides. In the current paper, we report a three-dimensional quantitative structure–activity relationship (3D-QSAR) study on 1-(substituted phenoxyacetoxy)alkylphosphonate using comparative molecular field analysis (CoMFA) (22) and comparative molecular similarity indices analysis (CoMSIA) models (23). To further explore the probable binding site of PDHc E1, a flexible molecular docking approach was carried out and the docking conformations were assumed to be the actual bioactive binding conformations. Mapping the 3D-QSAR models with the 3D topology of active site of PDHc E1 shows that the spatial and the electronic distributions of ligand-based models match well with those of the active site of the receptor, which provides further insight into the of enzyme–inhibitor interaction mechanism. The binding model proposed herein is valuable and applicable in the further research and development of novel potent PDHc E1 targeted inhibitors.

MATERIALS AND METHODS

Reagents and General Synthetic Procedure. Chemicals and reagents were obtained from commercial sources, and all of the solvents were anhydrous. Column chromatography was carried out with Merck silica gel (230–400 mesh). Thin-layer chromatography was performed on silica gel GF-254. Melting points (mp) were measured on an Electrothermal melting point apparatus and were uncorrected. IR spectra were recorded as KBr pellets on a Perkin-Elmer Fourier transform infrared spectrophotometer; only the most significant absorption bands have been reported. ¹H NMR were recorded on Varian XL-400 spectrometer at 400 MHz, using tetramethylsilane as internal standard. Chemical shifts (δ) are given in ppm, coupling constants (*J*) are in Hz, and multiplicities are implicated by s (singlet), d (doublet), t (triplet), q (quartet), and m (multiplet). MS spectra were analyzed on a Finnigan TRACE spectrometer and API2000LC/MS. Elemental analyses were performed by a Vario EL III elemental analyzer. The results of elemental analyses for C, H, and N were within ±0.5% of the theoretical values.

All of the compounds (1–58) studied in this work were synthesized according to the methods described in the literature (11–15), in which compounds 19–31, 34, 37, 39–41, and 43–58 have been reported.

Data for *O,O*-Dimethyl (3-Fluorophenoxyacetoxy)(furan-2-yl)methylphosphonate (1). Yellowish liquid; 0.89 g; yield, 70%; *n*_D²⁰ 1.5238; *R*_f = 0.60 (silica gel, acetone/petroleum ether, 1:1). IR (KBr, cm⁻¹): 3054 (ArC–H), 1736 (C=O, str), 1596 (ArC–C), 1491 (ArC–C), 1459 (ArC–C), 1234, 1169, 1038, 939. ¹H NMR (CDCl₃): δ 3.72 (d, 3H, *J* = 10.8, OCH₃), 3.82 (d, 3H, *J* = 10.8, OCH₃), 4.67, 4.71 (q, AB system, 2H, *J*_{AB} = 16.5, OCH₂CO), 6.40 (d, 1H, *J* = 10.8, PCO), 6.43 (s, 1H, 3-furanyl-H), 6.63 (s, 1H, 4-furanyl-H), 6.81–6.89 (m, 3H, 2, 4 and 6-phenyl-H), 6.97 (m, 1H, 5-phenyl-H), 7.48 (s, 1H, 5-furanyl-H). EI-MS *m/z* (%): 358 (M⁺ 34), 205 (17), 189 (77), 170 (6), 125 (72), 112 (10), 109 (56), 95 (100), 93 (77). Anal. calcd for C₁₅H₁₆FO₇P: C, 50.29; H, 4.50. Found: C, 50.60; H, 4.39.

Data for *O,O*-Dimethyl (4-Fluorophenoxyacetoxy)(furan-2-yl)methylphosphonate (2). White solid; 0.82 g; yield, 65%; mp 69–71 °C; *R*_f = 0.62 (silica gel, acetone/petroleum ether, 1:1). IR (KBr, cm⁻¹): 3075 (ArC–H), 1777 (C=O, str), 1596 (ArC–C), 1502 (ArC–C), 1453 (ArC–C), 1247, 1177, 1055, 944. ¹H NMR (CDCl₃): δ 3.75 (d, 3H, *J* = 10.8, OCH₃), 3.81 (d, 3H, *J* = 10.8, OCH₃), 4.66, 4.69 (q, AB system, 2H, *J*_{AB} = 16.5, OCH₂CO), 6.38 (d, 1H, *J* = 11.1, PCO), 6.40 (s, 1H, 3-furanyl-H), 6.62–6.64 (m, 1H, 4-furanyl-H), 6.81–6.87 (m, 2H, 2 and 6-phenyl-H), 6.92–6.99 (m, 2H, 3 and 5-phenyl-H), 7.48 (dd, 1H, *J* = 1.5, *J* = 0.9, 5-furanyl-H). EI-MS *m/z* (%): 358 (M⁺ 16), 205 (24), 189 (57), 170 (54), 125 (92), 112 (34), 109 (23), 95 (100), 93 (57). Anal. calcd for C₁₅H₁₆FO₇P: C, 50.29; H, 4.50. Found: C, 50.72; H, 4.42.

Data for *O,O*-Dimethyl (4-Chlorophenoxyacetoxy)(furan-2-yl)methylphosphonate (3). White solid; 0.96 g; yield, 76%; mp 107–108 °C;

$R_f = 0.61$ (silica gel, acetone/petroleum ether, 1:1). IR (KBr, cm^{-1}): 3023 (ArC—H), 1777 (C=O, str), 1589 (ArC—C), 1494 (ArC—C), 1446 (ArC—C), 1255, 1171, 1037, 945. ^1H NMR (CDCl_3): δ 3.74 (d, 3H, $J = 10.8$, OCH_3), 3.77 (d, 3H, $J = 10.8$, OCH_3), 4.80 (s, 2H, OCH_2CO), 6.37 (d, 1H, $J = 13.8$, PCHO), 6.85 (dd, 2H, $J = 6.9$, $J = 2.4$, 2 and 6-phenyl-H), 7.23 (dd, 2H, $J = 6.9$, $J = 2.4$, 3 and 5-phenyl-H), 7.26–7.29 (m, 1H, 3-furanyl-H), 7.42 (d, 1H, $J = 7.8$, 4-furanyl-H), 7.71 (dd, 1H, $J = 7.8$, $J = 1.4$, 5-furanyl-H). EI-MS m/z (%): 374 ($\text{M}^+ 0.7$), 258 (20), 244 (77), 201 (22), 186 (13), 148 (10), 141 (26), 109 (43), 94 (8), 93 (58). Anal. calcd for $\text{C}_{15}\text{H}_{16}\text{ClO}_7\text{P}$: C, 48.08; H, 4.30. Found: C, 48.13; H, 4.37.

Data for *O,O*-Dimethyl (2,4-Dichlorophenoxyacetoxy)(furan-2-yl)methylphosphonate (4). Yellowish solid; 1.10 g; yield, 87%; mp 62–63 °C; $R_f = 0.60$ (silica gel, acetone/petroleum ether, 1:1). IR (KBr, cm^{-1}): 3074 (ArC—H), 1765 (C=O, str), 1583 (ArC—C), 1483 (ArC—C), 1439 (ArC—C), 1285, 1188, 1036, 934. ^1H NMR (CDCl_3): δ 3.76 (d, 3H, $J = 10.8$, OCH_3), 3.83 (d, 3H, $J = 10.8$, OCH_3), 4.75, 4.78 (q, AB system, 2H, $J_{AB} = 16.5$, OCH_2CO), 6.38 (d, 1H, $J = 14.8$, PCHO), 6.40–6.42 (m, 1H, 3-furanyl-H), 6.62 (t, 1H, $J = 2.4$, 4-furanyl-H), 6.75 (d, 1H, $J = 8.8$, 6-phenyl-H), 7.13 (dd, 1H, $J = 8.8$, $J = 2.4$, 5-phenyl-H), 7.37 (d, 1H, $J = 2.4$, 3-phenyl-H), 7.47 (t, 1H, $J = 0.9$, 5-furanyl-H). EI-MS m/z (%): 408 ($\text{M}^+ 13$), 220 (66), 205 (53), 189 (75), 175 (61), 162 (100), 145(32), 133 (37), 109 (50), 94 (6), 93 (70). Anal. calcd for $\text{C}_{15}\text{H}_{15}\text{Cl}_2\text{O}_7\text{P}$: C, 44.03; H, 3.70. Found: C, 44.08; H, 3.67.

Data for *O,O*-Dimethyl (2,6-Dichlorophenoxyacetoxy)(furan-2-yl)methylphosphonate (5). Yellowish solid; 0.76 g; yield, 60%; mp 92–93 °C; $R_f = 0.62$ (silica gel, acetone/petroleum ether, 1:1). IR (KBr, cm^{-1}): 3126, 1767 (C=O, str), 1567 (ArC—C), 1458 (ArC—C), 1428 (ArC—C), 1271, 1189, 1032, 937. ^1H NMR (CDCl_3): δ 3.79 (d, 3H, $J = 10.8$, OCH_3), 3.85 (d, 3H, $J = 10.8$, OCH_3), 4.71 (s, 2H, OCH_2CO), 6.41 (s, 1H, 3-furanyl-H), 6.44 (d, 1H, $J = 15.9$, PCHO), 6.65 (s, 1H, 4-furanyl-H), 6.98–7.03 (m, 1H, 4-phenyl-H), 7.26 (d, 2H, $J = 8.0$, 3 and 5-phenyl-H), 7.46 (s, 1H, 5-furanyl-H). EI-MS m/z (%): 408 ($\text{M}^+ 20$), 220 (40), 205 (11), 189 (98), 175 (32), 162 (100), 145(17), 133 (25), 109 (21), 94 (2), 93 (27). Anal. calcd for $\text{C}_{15}\text{H}_{15}\text{Cl}_2\text{O}_7\text{P}$: C, 44.03; H, 3.70. Found: C, 44.44; H, 3.48.

Data for *O,O*-Dimethyl (2,3-Dichlorophenoxyacetoxy)(furan-2-yl)methylphosphonate (6). Yellowish solid; 0.79 g; yield, 62%; mp 81–82 °C; $R_f = 0.64$ (silica gel, acetone/petroleum ether, 1:1). IR (KBr, cm^{-1}): 3081 (ArC—H), 1779 (C=O, str), 1581 (ArC—C), 1463 (ArC—C), 1427 (ArC—C), 1270, 1172, 1054, 938. ^1H NMR (CDCl_3): δ 3.75 (d, 3H, $J = 10.8$, OCH_3), 3.83 (d, 3H, $J = 10.8$, OCH_3), 4.79, 4.82 (q, AB system, 2H, $J_{AB} = 16.5$, OCH_2CO), 6.38 (d, 1H, $J = 11.4$, PCHO), 6.41 (s, 1H, 3-furanyl-H), 6.63 (d, 1H, $J = 1.5$, 4-furanyl-H), 6.98–7.03 (dd, 1H, $J = 5.4$, $J = 1.8$, 6-phenyl-H), 7.09–7.13 (m, 2H, 4 and 5-phenyl-H), 7.48 (s, 1H, 5-furanyl-H). EI-MS m/z (%): 408 ($\text{M}^+ 60$), 377 (11), 271 (20), 249 (34), 220 (20), 205 (92), 189 (98), 175 (90), 162 (38), 145(63), 133 (22), 109 (81), 94 (25), 93 (100). Anal. calcd for $\text{C}_{15}\text{H}_{15}\text{Cl}_2\text{O}_7\text{P}$: C, 44.03; H, 3.70. Found: C, 44.50; H, 3.50.

Data for *O,O*-Dimethyl (4-Chloro-2-methylphenoxyacetoxy)(furan-2-yl)methylphosphonate (7). Yellowish liquid; 1.00 g; yield, 79%; n_D^{20} 1.5016; $R_f = 0.63$ (silica gel, acetone/petroleum ether, 1:1). IR (KBr, cm^{-1}): 3078 (ArC—H), 1772 (C=O, str), 1598 (ArC—C), 1492 (ArC—C), 1447 (ArC—C), 1235, 1171, 1039, 932. ^1H NMR (CDCl_3): δ 2.25 (s, 3H, PhCH_3), 3.76 (d, 3H, $J = 11.0$, OCH_3), 3.81 (d, 3H, $J = 11.0$, OCH_3), 4.70, 4.73 (q, AB system, 2H, $J_{AB} = 16.5$, OCH_2CO), 6.39 (d, 1H, $J = 14.4$, PCHO), 6.40–6.42 (m, 1H, 3-furanyl-H), 6.52 (s, 1H, 4-furanyl-H), 6.62–6.66 (m, 1H, 6-phenyl-H), 7.06–7.08 (m, 1H, 5-phenyl-H), 7.13 (s, 1H, 3-phenyl-H), 7.45–7.49 (m, 1H, 5-furanyl-H). EI-MS m/z (%): 388 ($\text{M}^+ 17$), 234 (38), 205 (23), 189 (100), 165 (1), 155 (58), 142 (19), 125(51), 109 (46), 94 (9), 93 (67). Anal. calcd for $\text{C}_{16}\text{H}_{18}\text{ClO}_7\text{P}$: C, 49.43; H, 4.67. Found: C, 49.72; H, 4.52.

Data for *O,O*-Dimethyl (4-Chloro-3-methylphenoxyacetoxy)(furan-2-yl)methylphosphonate (8). White solid; 0.99 g; yield, 78%; mp 47–48 °C; $R_f = 0.60$ (silica gel, acetone/petroleum ether, 1:1). IR (KBr, cm^{-1}): 3081 (ArC—H), 1774 (C=O, str), 1576 (ArC—C), 1478 (ArC—C), 1447 (ArC—C), 1269, 1170, 1055, 939. ^1H NMR (CDCl_3): δ 2.31 (s, 3H, PhCH_3), 3.75 (d, 3H, $J = 10.7$, OCH_3), 3.80 (d, 3H, $J = 10.7$, OCH_3), 4.66, 4.69 (q, AB system, 2H, $J_{AB} = 16.4$, OCH_2CO), 6.38 (d, 1H, $J = 12.8$, PCHO), 6.40–6.42 (m, 1H, 3-furanyl-H), 6.61–6.67

(m, 2H, 2 and 6-phenyl-H), 6.76 (d, 1H, $J = 3.0$, 4-furanyl-H), 7.21 (d, 1H, $J = 8.8$, 5-phenyl-H), 7.48 (t, 1H, $J = 1.2$, 5-furanyl-H). EI-MS m/z (%): 388 ($\text{M}^+ 11$), 309 (57), 234 (29), 205 (49), 200 (49), 189 (100), 165 (10), 155 (86), 142 (41), 125(79), 109 (70), 94 (18), 93 (96). Anal. calcd for $\text{C}_{16}\text{H}_{18}\text{ClO}_7\text{P}$: C, 49.43; H, 4.67. Found: C, 49.53; H, 4.56.

Data for *O,O*-Dimethyl (2-Chloro-5-methylphenoxyacetoxy)(furan-2-yl)methylphosphonate (9). White solid; 0.81 g; yield, 64%; mp 97–98 °C; $R_f = 0.60$ (silica gel, acetone/petroleum ether, 1:1). IR (KBr, cm^{-1}): 3115, 1774 (C=O, str), 1585 (ArC—C), 1493 (ArC—C), 1448 (ArC—C), 1265, 1170, 1059, 930. ^1H NMR (CDCl_3): δ 2.27 (s, 3H, PhCH_3), 3.75 (d, 3H, $J = 10.8$, OCH_3), 3.82 (d, 3H, $J = 10.8$, OCH_3), 4.75, 4.78 (q, AB system, 2H, $J_{AB} = 16.5$, OCH_2CO), 6.39 (d, 1H, $J = 11.2$, PCHO), 6.39–6.42 (m, 1H, 3-furanyl-H), 6.60–6.63 (m, 2H, 4-furanyl-H and 6-phenyl-H), 6.73–6.77 (m, 1H, 4-phenyl-H), 7.23 (d, 1H, $J = 8.0$, 3-phenyl-H), 7.48 (t, 1H, $J = 0.9$, 5-furanyl-H). EI-MS m/z (%): 388 ($\text{M}^+ 1$), 205 (3), 200 (54), 189 (9), 165 (18), 155 (27), 142 (36), 125(44), 109 (12), 94 (6), 93 (12). Anal. calcd for $\text{C}_{16}\text{H}_{18}\text{ClO}_7\text{P}$: C, 49.43; H, 4.67. Found: C, 49.23; H, 4.47.

Data for *O,O*-Dimethyl (3-Fluorophenoxyacetoxy)(thien-2-yl)methylphosphonate (10). Yellowish solid; 0.89 g; yield, 70%; mp 76–77 °C; $R_f = 0.64$ (silica gel, acetone/petroleum ether, 1:1). IR (KBr, cm^{-1}): 3087 (ArC—H), 1740 (C=O, str), 1596 (ArC—C), 1491 (ArC—C), 1437 (ArC—C), 1213, 1143, 1040, 940. ^1H NMR (CDCl_3): δ 3.70 (d, 3H, $J = 10.8$, OCH_3), 3.77 (d, 3H, $J = 10.8$, OCH_3), 4.61 (s, 2H, OCH_2CO), 6.62–6.71 (m, 4H, PCHO , 2, 4 and 6-phenyl-H), 6.99 (t, 1H, $J = 3.0$, 3-thienyl-H), 7.14 (d, 1H, $J = 2.4$, 5-phenyl-H), 7.19–7.23 (m, 1H, 4-thienyl-H), 7.27–7.31 (m, 1H, 5-thienyl-H). EI-MS m/z (%): 374 ($\text{M}^+ 2$), 220 (11), 205 (21), 170 (36), 125 (47), 113 (50), 109 (40), 95 (100), 93 (20). Anal. calcd for $\text{C}_{15}\text{H}_{16}\text{FO}_6\text{PS}$: C, 48.13; H, 4.31. Found: C, 48.48; H, 4.14.

Data for *O,O*-Dimethyl (4-Fluorophenoxyacetoxy)(thien-2-yl)methylphosphonate (11). Yellowish solid; 0.85 g; yield, 67%; mp 68–70 °C; $R_f = 0.62$ (silica gel, acetone/petroleum ether, 1:1). IR (KBr, cm^{-1}): 3083 (ArC—H), 1762 (C=O, str), 1627 (ArC—C), 1506 (ArC—C), 1444 (ArC—C), 1247, 1195, 1029, 941. ^1H NMR (CDCl_3): δ 3.70 (d, 3H, $J = 10.7$, OCH_3), 3.77 (d, 3H, $J = 10.7$, OCH_3), 4.64, 4.67 (q, AB system, 2H, $J_{AB} = 16.4$, OCH_2CO), 6.54 (d, 1H, $J = 13.5$, PCHO), 6.80–6.83 (m, 2H, 2 and 6-phenyl-H), 6.91–6.93 (m, 2H, 3 and 5-phenyl-H), 6.99–7.03 (m, 1H, 3-thienyl-H), 7.27–7.31 (m, 1H, 4-thienyl-H), 7.38 (d, 1H, $J = 5.2$, 5-thienyl-H). EI-MS m/z (%): 374 ($\text{M}^+ 51$), 220 (14), 205 (100), 170 (17), 125 (84), 113 (31), 109 (51), 94 (24), 93 (85). Anal. calcd for $\text{C}_{15}\text{H}_{16}\text{FO}_6\text{PS}$: C, 48.13; H, 4.31. Found: C, 48.30; H, 4.19.

Data for *O,O*-Dimethyl (2,4-Dichlorophenoxyacetoxy)(thien-2-yl)methylphosphonate (12). Yellowish solid; 1.15 g; yield, 91%; mp 92–93 °C; $R_f = 0.62$ (silica gel, acetone/petroleum ether, 1:1). IR (KBr, cm^{-1}): 3072 (ArC—H), 1763 (C=O, str), 1582 (ArC—C), 1483 (ArC—C), 1434 (ArC—C), 1275, 1190, 1038, 946. ^1H NMR (CDCl_3): δ 3.70 (d, 3H, $J = 10.5$, OCH_3), 3.77 (d, 3H, $J = 10.5$, OCH_3), 4.74, 4.77 (q, AB system, 2H, $J_{AB} = 16.5$, OCH_2CO), 6.50 (d, 1H, $J = 13.5$, PCHO), 6.69 (d, 1H, $J = 8.8$, 6-phenyl-H), 6.98–7.01 (t, 1H, $J = 3.6$, 3-thienyl-H), 7.24 (s, 1H, 4-thienyl-H), 7.09 (dd, 1H, $J = 8.8$, $J = 2.4$, 5-phenyl-H), 7.35–7.36 (m, 2H, 3-phenyl-H and 5-thienyl-H). EI-MS m/z (%): 424 ($\text{M}^+ 9$), 220 (37), 205 (60), 175 (58), 162 (76), 145 (26), 133 (28), 109 (33), 94 (4), 93 (100). Anal. calcd for $\text{C}_{15}\text{H}_{15}\text{Cl}_2\text{O}_6\text{PS}$: C, 42.37; H, 3.56. Found: C, 42.47; H, 3.90.

Data for *O,O*-Dimethyl (4-Chlorophenoxyacetoxy)(thien-2-yl)methylphosphonate (13). Yellowish solid; 1.08 g; yield, 85%; mp 94–95 °C; $R_f = 0.61$ (silica gel, acetone/petroleum ether, 1:1). IR (KBr, cm^{-1}): 3083 (ArC—H), 1762 (C=O, str), 1596 (ArC—C), 1494 (ArC—C), 1443 (ArC—C), 1247, 1177, 1027, 939. ^1H NMR (CDCl_3): δ 3.71 (d, 3H, $J = 10.8$, OCH_3), 3.78 (d, 3H, $J = 10.8$, OCH_3), 4.67, 4.71 (q, AB system, 2H, $J_{AB} = 16.4$, OCH_2CO), 6.53 (d, 1H, $J = 13.5$, PCHO), 6.77–6.82 (m, 2H, 2 and 6-phenyl-H), 7.00–7.04 (m, 1H, 3-thienyl-H), 7.19–7.24 (m, 2H, 3 and 5-phenyl-H), 7.26–7.30 (m, 1H, 4-thienyl-H), 7.39 (d, 1H, 5-thienyl-H). EI-MS m/z (%): 390 ($\text{M}^+ 31$), 220(31), 205 (74), 186 (9), 141 (54), 128 (20), 111 (62), 109 (63), 94 (18), 93 (100). Anal. calcd for $\text{C}_{15}\text{H}_{16}\text{ClO}_6\text{PS}$: C, 46.10; H, 4.13. Found: C, 46.01; H, 4.08.

Data for *O,O*-Dimethyl (2,6-Dichlorophenoxyacetoxy)(thien-2-yl)methylphosphonate (14). Yellowish solid; 0.94 g; yield, 74%; mp 78–79 °C; R_f = 0.61 (silica gel, acetone/petroleum ether, 1:1). IR (KBr, cm^{-1}): 3083 (ArC–H), 1767 (C=O, str), 1568 (ArC–C), 1457 (ArC–C), 1429 (ArC–C), 1273, 1180, 1037, 932. ^1H NMR (CDCl_3): δ 3.76 (d, 3H, J = 10.8, OCH_3), 3.82 (d, 3H, J = 10.8, OCH_3), 4.70, 4.74 (q, AB system, 2H, J_{AB} = 16.5, OCH_2CO), 6.62 (d, 1H, J = 10.2, PCHO), 7.03–7.06 (m, 2H, 3-thienyl-H and 4-phenyl-H), 7.27–7.33 (m, 3H, 4-thienyl-H, 3 and 5-phenyl-H), 7.39 (d, 1H, J = 3.6, 5-thienyl-H). EI-MS m/z (%): 424 (M^+ 14), 220 (41), 205 (50), 175 (89), 162 (100), 145 (23), 133 (26), 109 (36), 94 (3), 93 (86). Anal. calcd for $\text{C}_{15}\text{H}_{15}\text{Cl}_2\text{O}_6\text{PS}$: C, 42.37; H, 3.56. Found: C, 41.93; H, 3.49.

Data for *O,O*-Dimethyl (2,3-Dichlorophenoxyacetoxy)(thien-2-yl)methylphosphonate (15). Yellowish solid; 0.91 g; yield, 72%; mp 108–110 °C; R_f = 0.62 (silica gel, acetone/petroleum ether, 1:1). IR (KBr, cm^{-1}): 3080 (ArC–H), 1781 (C=O, str), 1580 (ArC–C), 1466 (ArC–C), 1431 (ArC–C), 1256, 1178, 1038, 945. ^1H NMR (CDCl_3): δ 3.71 (d, 3H, J = 10.8, OCH_3), 3.79 (d, 3H, J = 10.8, OCH_3), 4.79, 4.82 (q, AB system, 2H, J_{AB} = 16.5, OCH_2CO), 6.54 (d, 1H, J = 13.5, PCHO), 6.69 (d, 1H, J = 5.7, 6-phenyl-H), 7.01–7.03 (m, 1H, 3-thienyl-H), 7.09–7.13 (m, 2H, J = 1.5, 4 and 5-phenyl-H), 7.27–7.28 (m, 1H, 4-thienyl-H), 7.38–7.40 (m, 1H, 5-thienyl-H). EI-MS m/z (%): 424 (M^+ 3), 220 (62), 205 (4), 175 (40), 162 (69), 145 (35), 133 (31), 109 (37), 94 (5), 93 (14). Anal. calcd for $\text{C}_{15}\text{H}_{15}\text{Cl}_2\text{O}_6\text{PS}$: C, 42.37; H, 3.56. Found: C, 42.77; H, 3.63.

Data for *O,O*-Dimethyl (4-Chloro-2-methylphenoxyacetoxy)(thien-2-yl)methylphosphonate (16). Yellowish solid; 1.09 g; yield, 86%; mp 80–81 °C; R_f = 0.64 (silica gel, acetone/petroleum ether, 1:1). IR (KBr, cm^{-1}): 3079 (ArC–H), 1783 (C=O, str), 1599 (ArC–C), 1495 (ArC–C), 1441 (ArC–C), 1259, 1169, 1028, 949. ^1H NMR (CDCl_3): δ 2.25 (s, 3H, PhCH_3), 3.71 (d, 3H, J = 10.4, OCH_3), 3.77 (d, 3H, J = 10.4, OCH_3), 4.70, 4.74 (q, AB system, 2H, J_{AB} = 16.5, OCH_2CO), 6.51–6.57 (m, 2H, PCHO and 6-phenyl-H), 7.02–7.04 (m, 2H, 3-thienyl-H and 3-phenyl-H), 7.13 (d, 1H, J = 1.6, 5-phenyl-H), 7.27 (s, 1H, 4-thienyl-H), 7.39 (d, 1H, J = 3.6, 5-thienyl-H). EI-MS m/z (%): 404 (M^+ 17), 250 (20), 219 (8), 205 (84), 200 (5), 155 (65), 142 (11), 125 (70), 109 (60), 94 (5), 93 (100). Anal. calcd for $\text{C}_{16}\text{H}_{18}\text{ClO}_6\text{PS}$: C, 47.47; H, 4.48. Found: C, 47.70; H, 4.48.

Data for *O,O*-Dimethyl (4-Chloro-3-methylphenoxyacetoxy)(thien-2-yl)methylphosphonate (17). Yellowish solid; 1.11 g; yield, 88%; mp 74–75 °C; R_f = 0.63 (silica gel, acetone/petroleum ether, 1:1). IR (KBr, cm^{-1}): 3076 (ArC–H), 1766 (C=O, str), 1599 (ArC–C), 1489 (ArC–C), 1435 (ArC–C), 1249, 1174, 1027, 928. ^1H NMR (CDCl_3): δ 2.30 (s, 3H, PhCH_3), 3.70 (d, 3H, J = 10.8, OCH_3), 3.78 (d, 3H, J = 10.8, OCH_3), 4.66, 4.70 (q, AB system, 2H, J_{AB} = 16.5, OCH_2CO), 6.53 (d, 1H, J = 13.5, PCHO), 6.62–6.66 (m, 1H, 2-phenyl-H), 6.74 (d, 1H, 6-phenyl-H), 7.00–7.04 (m, 1H, 3-thienyl-H), 7.20 (d, 1H, J = 8.8, 5-phenyl-H), 7.26–7.29 (m, 1H, 4-thienyl-H), 7.37 (m, 1H, 5-thienyl-H). EI-MS m/z (%): 404 (M^+ 13), 369 (26), 325 (61), 250 (26), 219 (46), 205 (100), 200 (44), 155 (86), 142 (37), 125 (75), 109 (60), 94 (17), 93 (99). Anal. calcd for $\text{C}_{16}\text{H}_{18}\text{ClO}_6\text{PS}$: C, 47.47; H, 4.48. Found: C, 47.19; H, 4.46.

Data for *O,O*-Dimethyl (2-Chloro-5-methylphenoxyacetoxy)(thien-2-yl)methylphosphonate (18). Yellowish solid; 1.09 g; yield, 86%; mp 90–91 °C; R_f = 0.60 (silica gel, acetone/petroleum ether, 1:1). IR (KBr, cm^{-1}): 3109, 1769 (C=O, str), 1584 (ArC–C), 1493 (ArC–C), 1433 (ArC–C), 1263, 1171, 1030, 936. ^1H NMR (CDCl_3): δ 2.25 (s, 3H, PhCH_3), 3.72 (d, 3H, J = 10.6, OCH_3), 3.78 (d, 3H, J = 10.6, OCH_3), 4.75, 4.79 (q, AB system, 2H, J_{AB} = 16.5, OCH_2CO), 6.54 (d, 1H, J = 13.5, PCHO), 6.59 (d, 1H, J = 1.2, 6-phenyl-H), 6.74 (dd, 1H, J = 8.0, J = 1.2, 4-phenyl-H), 7.02 (dd, 1H, J = 4.5, J = 3.6, 3-thienyl-H), 7.24 (d, 1H, J = 8.0, 3-phenyl-H), 7.26–7.29 (m, 1H, 4-thienyl-H), 7.36–7.38 (m, 1H, 5-thienyl-H). EI-MS m/z (%): 404 (M^+ 1), 220 (14), 205 (93), 200 (100), 155 (91), 142 (67), 125 (64), 109 (19), 94 (3), 93 (75). Anal. calcd for $\text{C}_{16}\text{H}_{18}\text{ClO}_6\text{PS}$: C, 47.47; H, 4.48. Found: C, 47.42; H, 4.59.

Data for Sodium *O*-Methyl (2,4-Dichlorophenoxyacetoxy)(furan-2-yl)methylphosphonate (32). Yellowish solid; 1.20 g; yield, 95%; mp 99–100 °C. IR (KBr, cm^{-1}): 3104, 1742 (C=O, str), 1646 (ArC–C), 1601 (ArC–C), 1485 (ArC–C), 1216, 1078, 1053, 938. ^1H NMR (DMSO- d_6): δ 3.36 (d, 3H, J = 10.0, OCH_3), 4.89, 4.94 (q, AB system,

2H, J_{AB} = 16.5, OCH_2CO), 5.88 (d, 1H, J = 12.0, PCHO), 6.38 (s, 1H, 3-furanyl-H), 6.53 (s, 1H, 4-furanyl-H), 7.02 (d, 1H, J = 8.0, 6-phenyl-H), 7.29 (d, 1H, J = 8.0, 5-phenyl-H), 7.54 (s, 2H, 5-furanyl-H and 3-phenyl-H). EI-MS m/z (%): 416 (M^+ 0.1), 234 (6), 220 (43), 199 (13), 175 (2), 174 (35), 164 (100), 145 (26), 132 (36), 110 (37), 108 (36), 96 (10), 94 (2). ESI-MS m/z (%): 435 ($\text{M} + \text{Na}^+$) (100), 416 (M^+) (8), 393 ($\text{M} - \text{Na}^+$) (100). Anal. calcd for $\text{C}_{14}\text{H}_{12}\text{Cl}_2\text{NaO}_7\text{P}$: C, 40.31; H, 2.90. Found: C, 40.06; H, 2.96.

Data for Sodium *O*-Methyl (2,4-Dichlorophenoxyacetoxy)(pyridin-2-yl)methylphosphonate (33). Yellowish solid; 1.11 g; yield, 88%; mp 238 °C (dec). IR (KBr, cm^{-1}): 3160, 1730 (C=O, str), 1649 (ArC–C), 1584 (ArC–C), 1485 (ArC–C), 1249, 1084, 1052, 924. ^1H NMR (DMSO- d_6): δ 3.34 (d, 3H, J = 8.0, OCH_3), 5.00, 5.04 (q, AB system, 2H, J_{AB} = 16.5, OCH_2CO), 5.85 (d, 1H, J = 14.0, PCHO), 7.10 (d, 1H, J = 6.6, 6-phenyl-H), 7.13–7.16 (m, 1H, 5-pyridinyl-H), 7.28 (d, 1H, J = 6.6, 5-phenyl-H), 7.47 (d, 1H, J = 5.7, 3-pyridinyl-H), 7.52 (s, 1H, 3-phenyl-H), 7.65–7.68 (m, 1H, 4-pyridinyl-H), 8.45 (s, 1H, 6-pyridinyl-H). EI-MS m/z (%): 427 (M^+ 0.3), 234 (80), 220 (72), 199 (100), 175 (91), 162 (84), 145 (78), 133 (79), 111 (74), 109 (70), 107 (81), 98 (66), 94 (10), 93 (65). Anal. calcd for $\text{C}_{15}\text{H}_{13}\text{Cl}_2\text{NNaO}_6\text{P}$: C, 42.08; H, 3.06; N, 3.27. Found: C, 42.53; H, 3.06; N, 3.26.

Data for Sodium *O*-Methyl (2,4-Dichlorophenoxyacetoxy)(2-chlorophenyl)methylphosphonate (35). Yellowish solid; 0.89 g; yield, 70%; mp 130–131 °C. IR (KBr, cm^{-1}): 3006, 1746 (C=O, str), 1631 (ArC–C), 1560 (ArC–C), 1484 (ArC–C), 1238, 1078, 1051, 928. ^1H NMR (DMSO- d_6): δ 3.36 (d, 3H, J = 10.0, OCH_3), 4.93, 4.97 (q, AB system, 2H, J_{AB} = 16.5, OCH_2CO), 6.17 (d, 1H, J = 14.0, PCHO), 6.97 (d, 1H, J = 10.0, phenyl-H), 7.19–7.33 (m, 4H, phenyl-H), 7.58–7.62 (m, 2H, phenyl-H). EI-MS m/z (%): 460 (M^+ 0.5), 234 (32), 220 (14), 199 (58), 175 (45), 162 (100), 145 (25), 135 (61), 133 (28), 111 (31), 109 (24), 98 (33), 93 (2). Anal. calcd for $\text{C}_{16}\text{H}_{13}\text{Cl}_3\text{NaO}_6\text{P}$: C, 41.63; H, 2.84. Found: C, 41.88; H, 3.02.

Data for Sodium *O*-Methyl (2,4-Dichlorophenoxyacetoxy)(4-chlorophenyl)methylphosphonate (36). Yellowish solid; 0.90 g; yield, 71%; mp 141–142 °C. IR (KBr, cm^{-1}): 3098, 1727 (C=O, str), 1664 (ArC–C), 1590 (ArC–C), 1485 (ArC–C), 1240, 1088, 1056, 931. ^1H NMR (DMSO- d_6): δ 3.34 (d, 3H, J = 9.8, OCH_3), 4.94, 4.98 (q, AB system, 2H, J_{AB} = 16.5, OCH_2CO), 6.16 (d, 1H, J = 12.0, PCHO), 7.00 (d, 1H, J = 6.0, phenyl-H), 7.22–7.35 (m, 5H, phenyl-H), 7.57–7.62 (m, 2H, phenyl-H). ESI-MS m/z (%): 460 (M^+ 0.3), 234 (16), 220 (9), 199 (29), 175 (36), 162 (29), 149 (25), 145 (56), 133 (69), 111 (68), 109 (87), 98 (16), 93 (11). Anal. calcd for $\text{C}_{16}\text{H}_{13}\text{Cl}_3\text{NaO}_6\text{P}$: C, 41.63; H, 2.84. Found: C, 41.16; H, 2.66.

Data for Sodium *O*-Methyl (2,4-Dichlorophenoxyacetoxy)(3,4-dichlorophenyl)methyl phosphonate (38). Yellowish solid; 0.93 g; yield, 73%; mp 143–145 °C. IR (KBr, cm^{-1}): 3089 (ArC–H), 1727 (C=O, str), 1660 (ArC–C), 1585 (ArC–C), 1485 (ArC–C), 1240, 1087, 1056, 932. ^1H NMR (DMSO- d_6): δ 3.57 (d, 3H, J = 10.2, OCH_3), 4.89, 4.92 (q, AB system, 2H, J_{AB} = 16.6, OCH_2CO), 6.47 (d, 1H, J = 12.6, PCHO), 6.93 (d, 1H, J = 8.8, phenyl-H), 7.15–7.21 (m, 1H, phenyl-H), 7.27 (dd, 1H, J = 8.8, J = 2.7, phenyl-H), 7.39–7.42 (m, 1H, phenyl-H), 7.58 (dd, 1H, J = 8.4, J = 1.8, phenyl-H). EI-MS m/z (%): 494 (M^+ 0.8), 234 (25), 220 (19), 199 (30), 175 (61), 162 (100), 145 (11), 133 (19), 119 (11), 111 (52), 109 (36), 98 (31), 93 (10). Anal. calcd for $\text{C}_{16}\text{H}_{12}\text{Cl}_4\text{NaO}_6\text{P}$: C, 38.74; H, 2.44. Found: C, 38.44; H, 2.53.

Data for Sodium *O*-Methyl (2,4-Dichlorophenoxyacetoxy)(4-methylphenyl)methylphosphonate (42). Yellowish solid; 0.99 g; yield, 78%; mp 108 °C (dec). IR (KBr, cm^{-1}): 3076 (ArC–H), 1746 (C=O, str), 1643 (ArC–C), 1587 (ArC–C), 1485 (ArC–C), 1217, 1079, 1051, 950. ^1H NMR (DMSO- d_6): δ 2.25 (s, 3H, PhCH_3), 3.33 (d, 3H, J = 8.0, OCH_3), 4.98 (s, 2H, OCH_2CO), 5.79 (d, 1H, J = 12.0, PCHO), 7.03–7.22 (m, 3H, phenyl-H), 7.22–7.26 (m, 3H, phenyl-H), 7.51 (s, 1H, phenyl-H). EI-MS m/z (%): 440 (M^+ 0.8), 234 (25), 220 (19), 199 (30), 175 (61), 162 (100), 133 (19), 119 (11), 109 (36), 94 (4), 93 (10). Anal. calcd for $\text{C}_{17}\text{H}_{16}\text{Cl}_2\text{NaO}_6\text{P}$: C, 46.28; H, 3.66. Found: C, 46.75; H, 4.06.

X-ray Diffraction. Colorless blocks of compound **12** (0.10 mm \times 0.25 mm \times 0.3 mm) were mounted on a quartz fiber with protection oil. Cell dimensions and intensities were measured at 293 K on a Bruker SMART CCD area detector diffractometer with graphite-monochro-

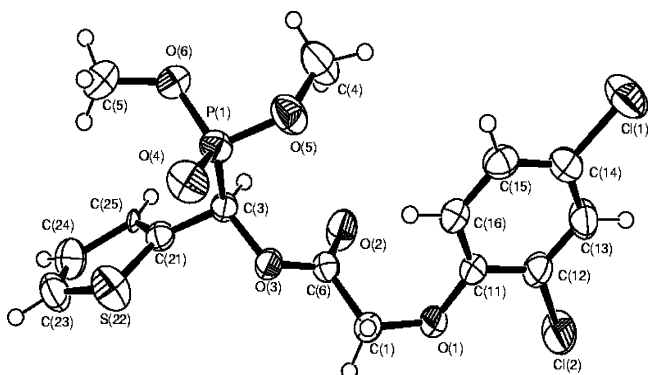


Figure 1. Molecular structure of compound 12.

Table 2. Crystal Data of Compound 12

space group	P2(1)/c
cell system	monoclinic
a, b, c (Å)	8.544, 17.54, 12.62
α , β , γ (°)	90.000, 98.963, 90.000
V (Å ³)	1867.8
Z	7
Dc (mg/m ³)	1.512
μ (mm ⁻¹)	0.573

mated Mo K α radiation ($\lambda = 0.71073$ Å); $\theta_{\max} = 25.03$; 7622 independent reflections ($R_{\text{int}} = 0.0282$) of which 3294 contributing reflections had $I > 2\sigma(I)$. The structure was solved by direct methods using SHELXS-97; all other calculations were performed with Bruker SAINT system and Bruker SMART programs. Full-matrix least-squares refinement gave final values of $R = 0.0646$, $\omega R = 0.1954$. Max/min residual electron density = $1.281/-0.851$ e Å⁻³. Hydrogen atoms were observed and refined with a fixed value of their isotropic displacement parameter. The molecular structure of compound 12 is shown in Figure 1, and a summary of data collection statistics is given in Table 2.

Herbicidal Activity Inhibition Assay. Dicotyledonous cucumber seeds, *Cucumis sativus* L., were chosen as tested plant materials because the title compounds showed higher herbicidal activities against dicotyledonous weeds. The herbicidal activity was measured according to the modified method described previously (24, 25). A set amount of each sample was dissolved in acetone to which a drop of an emulsifier, Tween 80, was added. The solution was then diluted with water until it reached the concentrations required. The amounts of acetone and the emulsifier were set as low as possible but still sufficient to make a uniform emulsion even at high concentrations. Five milliliters of solution was placed on a filter paper (diameter = 5.5 cm) in Petri dishes (diameter = 9.0 cm), and 10 cucumber seeds were placed on the filter paper after soaking in water for 6 h. The Petri dishes were kept at 28 °C for 3 days with 10 h of lighting and 14 h in the dark. After incubation for 72 h, the inhibition percentage was calculated by corresponding control using the length of the taproot as the indicator. Three replications per concentration were performed. According to the average percentage of inhibition of cucumber root at five or six concentrations for each test compound, the IC₅₀ was estimated by regression analysis using the logarithm of concentration and probit of the corresponding inhibition percentage.

Molecular Docking. Conventionally, CoMFA and CoMSIA are ligand-based modeling, which cannot ensure that the various field distributions of bioactivity predicting models match well with those of the active site of the real target enzyme. To make our 3D-QSAR predicting models more relevant to the real active site of the enzyme and to further explore a probable binding site in the PDHc E1, the most potent compound 12 was chosen as a standard template and docked into the active site of PDHc E1 proposed in the crystallographic studies (19, 20). To determine the probable active conformation that is employed as a template in 3D-QSAR studies, we used the advanced docking program AutoDock 3.0 (26) to dock the most potent compound 12 into the active site of the target enzyme. All molecular modeling calculations were performed using the SYBYL program (27), package

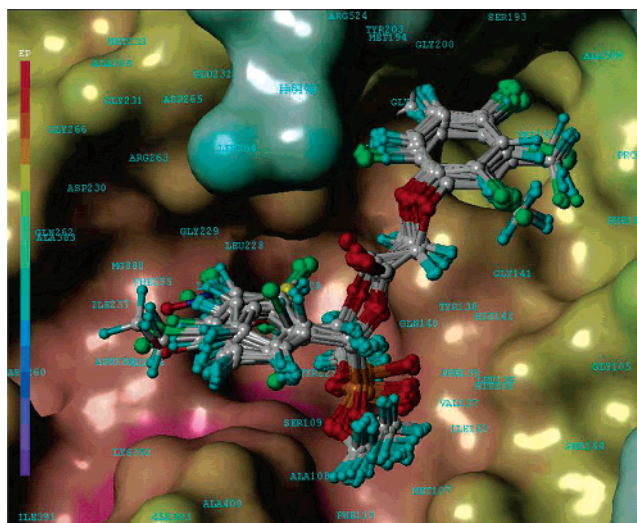


Figure 2. Probable binding conformations of the title compounds displayed inside the active site of the PDHc E1. This image was generated with the MOLCAD program in SYBYL 7.0, with some residues removed for clear visualization. The enzyme surface was rendered with electrostatic potential.

version 7.0, on a bioinformatics grid computer system. To select initial conformations of compounds, we used X-ray crystallographic coordinates of the highest active compound 12. The structure of PDHc E1 protein (PDB code 1L8A) (19) was obtained from the Protein Data Bank. The water molecules were removed, and polar hydrogen was added. The geometries of these compounds were subsequently optimized using the Tripos force field (28). The Powell method (29) was used for energy minimization with an energy convergence gradient value of 0.001 kcal/mol. The Kollman unit-atom charges were assigned to protein atoms using SYBYL 7.0.

The automated molecular docking calculations were carried out using AutoDock 3.0. The AUTOTORS module of AutoDock defined the active torsions for each docked compound. The active site of the protein was defined using AutoGrid. The grid map with $70 \times 70 \times 70$ points centered at the center of mass of the ThDP and a grid spacing of 0.375 Å was calculated using the AutoGrid program to evaluate the binding energies between the inhibitors and the protein. The Lamarckian genetic algorithm (LGA) (30) was used as a search method. Each LGA job consisted of 50 runs, and the number of generation in each run was 27000 with an initial population of 100 individuals. The step size was set to 0.2 Å for translation and 5° for orientation and torsion. The maximum number of energy evaluations was set to 1000000. Operator weights for cross-over, mutation, and elitism were 0.80, 0.02, and 1, respectively. The docked complexes of the inhibitor–enzyme were selected according to the criterion of interaction energy combined with geometrical and electronic matching quality.

Molecular Alignment and 3D-QSAR Modeling. The complexes were energetically minimized with only the inhibitor and the side-chain atoms of the protein to be flexible. Energy minimizations were carried out using SYBYL 7.0. In each step, the MMFF94 force field was used with 0.01 kcal/Å convergence and 5000 steps using the Powell method. The refined binding conformation of compound 12 was used for the 3D-QSAR studies. A database of the energy-minimized structures of 1–58 was aligned using the “align database” option of SYBYL with the compound 12 as the template of the alignment. Asterisks in the structural formula as shown in the top of Table 1 indicate the atoms (P and O) used for the alignments, and the final alignments are shown in Figure 2.

For 3D-QSAR analyses, 47 compounds were selected as a training set for model construction, and the rest of the 11 compounds (footnoted molecules in Table 1) as test set for model validation. The method for selection of test set in this study was fixed interval-sampling method. We randomly selected the #5 molecule in the molecular spreadsheet as a starting point. Then, any molecules with the number of $5n + 5$ ($n = 1, 2, 3, \dots, 11$) would be included in the test set.

CoMFA and CoMSIA Modeling. The steric and electrostatic potential fields for CoMFA were calculated at each lattice intersection of a regularly spaced grid of 2.0 Å. The lattice was defined automatically and was extended 4 Å units past Van der Waals volume of all molecules in X, Y, and Z directions. An sp^3 carbon atom with Van der Waals radius of 1.52 Å and +1.0 charge served as the probe atom to calculate steric (Lennard-Jones 6–12 potential) field energies and electrostatic (Coulombic potential) fields with a distance-dependent dielectric at each lattice point. The steric and electrostatic contributions were truncated to 30.0 kcal/mol, and electrostatic contributions were ignored at lattice intersections with maximum steric interactions. The CoMFA steric and electrostatic fields generated were scaled by CoMFA standard option given in SYBYL.

CoMSIA similarity indices descriptors were derived according to Klebe et al. (23) with the same lattice box as was used for the CoMFA. CoMSIA similarity indices (A_F) for a molecule j with atoms i at a grid point q were determined as follows:

$$A_{F,ik}^q(j) = \sum_i \omega_{\text{probe},k} \omega_{ik} e^{-\alpha r_{iq}^2}$$

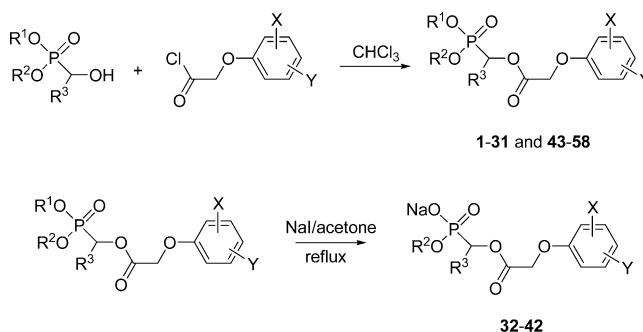
where ω_{ik} is the actual value of the physicochemical property k of atom i ; $\omega_{\text{probe},k}$ is the probe atom with a charge of +1, radius of 1 Å, hydrophobicity of +1, hydrogen bond donating of +1, and hydrogen bond accepting of +1; and r_{iq} is the mutual distance between the probe atom at grid point q and the atom i of the molecule. A Gaussian type distance dependence was considered between the grid point q and each atom i of the molecule, where r represents the distance. The default value of 0.3 was used as the attenuation factor (α). A lattice of 2 Å grid spacing was generated automatically.

Partial Least-Square (PLS) Calculations and Validations. PLS methodology was used for all 3D-QSAR analyses (31–33), in which the CoMFA and CoMSIA descriptors were used as independent variables and pIC_{50} values were used as dependent variables. The cross-validation with leave-one-out (LOO) option and the SAMPLS program (34), rather than column filtering, were carried out to obtain the optimum number of components to be used in the final analysis. The number of components used was not greater than one-third of the number (47) of rows in the training set. After the optimum number of components (N) was determined, a non-cross-validated analysis was performed without column filtering. The cross-validated correlation coefficient q^2 , standard error of prediction (SEP), non-cross-validated correlation coefficient r^2 , and F values and standard error of estimate (SE) values were computed according to the definitions in SYBYL. To further assess the robustness and statistical confidence of the derived models, bootstrapping analysis (100 runs) was performed, and the mean r^2 was given as the bootstrap (r_{bs}^2).

RESULTS AND DISCUSSION

Chemical Synthesis and Spectroscopic Analysis. Detailed synthetic methods of compounds **19–31**, **34**, **37**, **39–41**, and **43–58** have been reported elsewhere (11–15), and some additional new compounds with different substitution patterns have been designed and synthesized according to method in **Scheme 1**. The desired *O,O*-dimethyl 1-(substituted phenoxyacetoxy)alkylphosphonates **1–31** and **43–58** were obtained by reacting 2-phenoxyethanoyl chloride with corresponding 1-hydroxyalkylphosphonates in trichloromethane. A series of monosodium 1-(substituted phenoxyacetoxy)alkylphosphonates **32–42** were synthesized by the reaction of corresponding *O,O*-dimethyl 1-(substituted phenoxyacetoxy)alkylphosphonates with NaI in acetone under reflux. The reactions were carried out under nitrogen atmosphere to avoid hydrolysis of carboxylate ester group by atmosphere moisture. Most of title compounds have been evaluated against some monocotyledonous and dicotyledonous plants at a dose of 1.5 kg/ha in a greenhouse, and they showed a notable inhibitory effect against dicotyledonous plants for pre-emergence or postemergence. To carry out

Scheme 1. Synthesis of the 1-(Substituted phenoxyacetoxy)-alkylphosphonates **1–58**



3D-QSAR studies, The IC_{50} values of the title compounds were examined for pre-emergence inhibitory activity against *C. sativa* L. (cucumber) at different concentrations based on the preliminary herbicidal activity test results. The structures and inhibitory activities pIC_{50} values of all of the compounds reported in this paper are listed in **Table 1**.

In *O,O*-dimethyl 1-(substituted phenoxyacetoxy)alkylphosphonates series, the proton signal corresponding to the two methoxy groups ($-OCH_3$) attached with phosphorus appears as two doublet at δ 3.75 \pm 0.05 and 3.81 \pm 0.05, respectively. The chemical shifts of the two methyl hydrogens differentiate due to the low rate of environmental exchange caused by the slow rotation of the P–C bond, and the magnetic nucleus phosphorus makes the signal of both methyls split into a doublet. In monosodium 1-(substituted phenoxyacetoxy)alkylphosphonates series, the signal of methyl protons appears as a doublet caused by the phosphorus nucleus, at δ 3.45 \pm 0.12. The signal corresponding to the methylene group ($-CH_2-$) flanked by the phenoxy group and carbonyl group appears as a quartet, the outside lines smaller in size, which belongs to the AB system with the difference in chemical shift between the two mutually coupled protons A and B, at 4.72 \pm 0.08 and 4.73 \pm 0.08 in the former series and at 4.94 \pm 0.06 and 4.98 \pm 0.06 in the latter series, respectively. However, at the extreme, when A and B have exactly the same chemical shift, the outside lines disappear, and the inside lines merge into a singlet, exemplified by compounds **3**, **5**, **10**, and **42**.

In the mass spectroscopic analysis of title compounds, the base peak was dominated by the protonated substituted phenoxy moiety. Apparently, the molecular ion (M^+) loses the substituted phenoxyethanoyl or phenoxyethoxy groups to give rise to the oxoalkylphosphonates or alkylphosphonates, respectively. The weak molecular ion peak could be observed in monosodium 1-(substituted phenoxyacetoxy)alkylphosphonates series; therefore, compound **32** was randomly chosen to analyze using the electrospray ionization (ESI) method, in which the molecular ion (M^+) and characteristic positive ions ($M + Na$) $^+$ and ($M - Na$) $^+$ are apparent.

Binding Conformational Analysis. The most important requirement for CoMFA and CoMSIA studies is that the 3D structures to be analyzed are aligned according to a suitable conformational template, which is assumed to be a “bioactive” conformation. To obtain probable binding conformation and binding mode, we briefly summarize here the most prominent effects of structural modifications on the herbicidal activities of ligands. The data in **Table 1** showed that the modification of the substituents (X and Y) on the benzene ring could make the greatest changes in herbicidal activities in each series in which R^3 is a phenyl, thienyl, furyl, or aliphatic groups, respectively. The most important sites for enhancing the

Table 3. CoMFA and CoMSIA Results

	CoMFA	CoMSIA
PLS statistics		
q^2	0.872	0.873
N	6	6
SEP	0.383	0.383
r^2	0.974	0.954
SE	0.172	0.229
F	251.512	139.278
field distribution (%)		
steric	42.7	8.8
electrostatic	57.3	40.9
hydrophobic	/	50.2
testing set		
r_{bs}^2	0.983	0.972
SD^b	0.005	0.011
r_{pred}^2	0.883	0.908

^a Bootstrapped correlation coefficient. ^b Bootstrapped standard deviation.

$$r_{\text{pred}}^2 = 1 - \frac{\sum (p_{50}^{\text{obsd}} - p_{50}^{\text{pred}})^2 / 2}{\sum (p_{50}^{\text{obsd}} - p_{50}^{\text{mean}})^2}$$

herbicidal activity were X and Y at 2- and 4-positions of benzene ring. The simultaneous presence of electronegative groups (chlorine or fluorine) at the 2- and 4-positions of the benzene ring was most favorable for herbicidal activity. The improvement of activity due to the presence of negative charge at these positions is assumed to be the result of electrostatic interactions between the electronegative chlorine or fluorine atoms and positively charged counterparts of the receptor, such as protonated nitrogen atoms on Lys, Arg, Pro, and His side chains. Taking this essential electronic matching quality into account, the most probable conformation was selected in the top 10 ranked conformations. Fortunately, only one conformation could satisfy the electronic matching quality, with electropositive amino acid residues His106 and His640 around 2 and 4-positions of phenyl, respectively.

Figure 2 depicts the probable binding conformations of 1-(substituted phenoxyacetoxy)alkylphosphonate derivatives in the binding pocket of the PDHc E1. All molecules were aligned based on the assumption that they bind to the target site in the same manner. It is apparent that all of the members of this series have similar binding characteristics. The main steric, electronic, and hydrophobic interactions between the inhibitors and the residues such as His106, Met107, Ala108, Ser109, Tyr177, Leu264, Lys392, Ala399, Ala400, Glu522, Tyr599, Glu636, His640, and TDP887 in the binding pocket could be observed.

CoMFA and CoMSIA Analysis. The results of CoMFA and CoMSIA analysis are summarized in **Table 3**. The CoMFA PLS analysis yielded a high cross-validated correlation coefficient q^2 of 0.872 with a SEP of 0.383. The non-cross-validated PLS analysis gave a conventional r^2 of 0.974 with a SE of 0.172. These values indicate a good statistical correlation and reasonable predictability of the CoMFA model. The steric field descriptors explain 42.7% of the variance, while the electrostatic descriptors explain 57.3%.

The CoMSIA analysis using steric, electrostatic, and lipophilic fields as descriptors gave a model with q^2 of 0.873 and r^2 of 0.954. The CoMSIA steric, electrostatic, and lipophilic fields explain variance of 8.8, 40.9, and 50.2%, respectively. This indicates that the hydrophobic interaction is a major factor to explain the field properties of synthesized compounds. Further attempts to combine the hydrogen bond fields with the standard steric, electrostatic, and lipophilic fields did not lead to any significant improvement ($q^2 = 0.869$, $r^2 = 0.952$). Indeed, because hydrophobic and electrostatic interactions dominate the

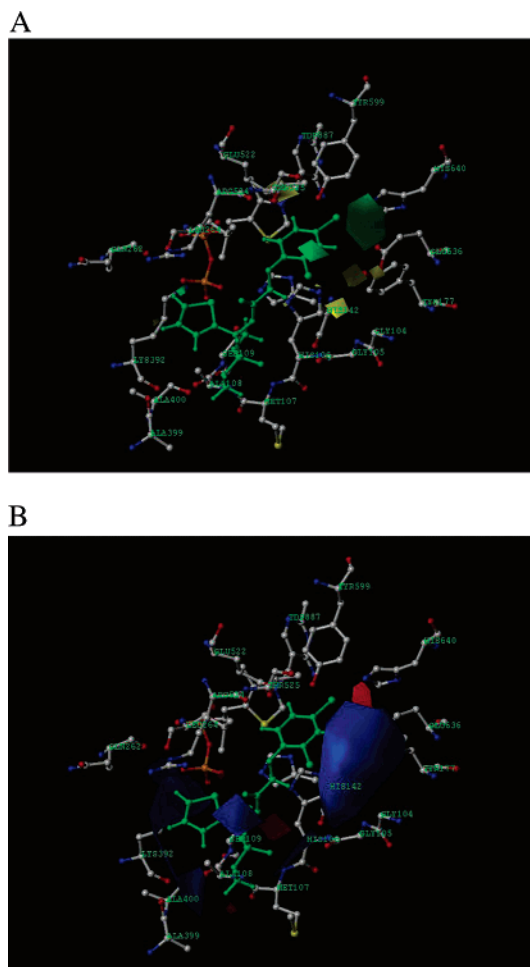


Figure 3. CoMFA contour maps displayed with compound **12** (green) and the key residues in the binding site of the PDHc E1. (A) Steric field distribution and (B) electrostatic field distribution. Sterically favored areas are in green; sterically disfavored areas are in yellow; positive potential favored areas are in blue; and positive potential disfavored areas in red.

inhibitor binding in PDHc E1, correlation coefficients between the activity and the hydrogen bond field are expected to be low. All of the results demonstrate that the CoMSIA model is also fairly predictive.

The steric contribution contour maps of CoMFA and CoMSIA are plotted in **Figures 3A** and **4A**, respectively. To aid in visualization, the most active compound **12** is displayed with a green color in the maps. The green and yellow polyhedra describe regions of space around the molecules where an increase in steric bulk enhances or diminishes the herbicidal activity, respectively. The CoMSIA approach provides more contiguous contour diagrams, which allows physicochemical properties relevant for binding to be mapped back onto the molecular structures. Furthermore, CoMSIA isocontour diagrams lie within regions occupied by the ligands, whereas CoMFA contours highlight those areas where the ligand would interact with a possible environment. Yet, the combined application of different approaches enables one to verify the convergence of the results, or the obtained conclusions can complement each other (35). In this case, the combination of CoMFA and CoMSIA methods leads to a better interpretation for QSAR at the 3D level.

The CoMFA sterically favorable green contours appear around the 4-position of the phenyl ring of compound **12**, suggesting that bulky groups in this region are favored for higher

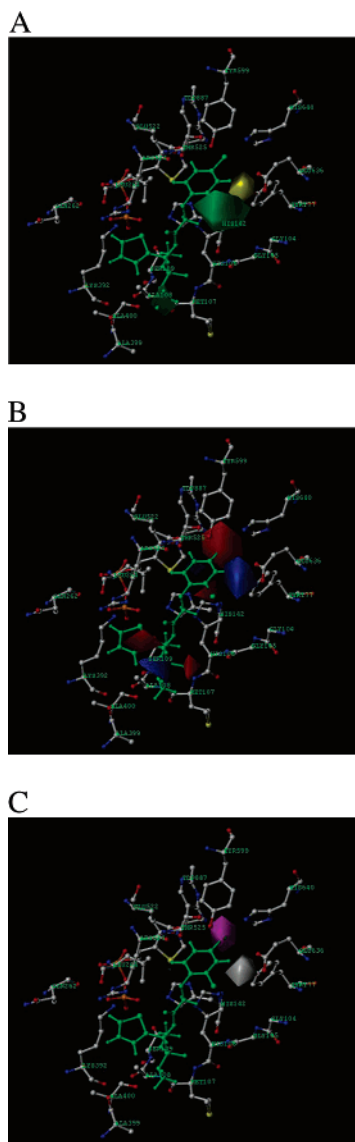


Figure 4. CoMSIA contour maps displayed with compound **12** (green) and the key residues in the binding site of the PDHc E1. (A) Steric field distribution, (B) electrostatic field distribution, and (C) hydrophobic field distribution. Sterically favored areas are in green; sterically unfavored areas are in yellow; positive potential favored areas are in blue; positive potential unfavored areas are in red; hydrophobic favored areas are in magenta; and hydrophilic favored areas are in white.

activity. This also can be seen with compounds **3**, **13**, **21**, **45**, and **53**, in which replacing 4-fluoro with 4-chloro results in a suitable increase of activity as compared to compounds **2**, **11**, **20**, **44**, and **52**. No significant increase in activity for compound **8**, **17**, **25**, **49**, and **57**, which bears an additional methyl group at the 3-position and overlaps with the CoMSIA sterically disfavored yellow region, were apparent. There is also a big region of green contour near the 2-position of phenyl (**Figure 4A**), indicating that more bulky substituents are needed in this position to improve the inhibitory activity. This is in agreement with the fact that the inhibitory activities of compounds **4**, **16**, **24**, and **56** with more bulky substituents are higher than those of compounds **3**, **13**, **21**, and **53**. However, in several yellow regions slightly above the 2-position of phenyl revealed by CoMFA analysis, it can be concluded that the size of the binding site is limited and there exists an optimal value for the steric effect. The prediction was confirmed by the alignment of

inhibitor and receptor, which was shown in **Figure 3A** that the residues Glu636, Tyr177, Tyr599, TDP887, Glu522, and Leu264 in the binding pocket of PDHc E1 are at distances of less than 3.0 Å corresponding to the substructure of the inhibitors. Therefore, a larger substitute than chlorine may lead to collision with the corresponding residues in the pocket.

The electrostatic contour plots are shown in **Figures 3B** and **4B**. As the same of steric maps, CoMFA and CoMSIA analyses reveal essentially complementary results here. The blue contour defines a region where increasing the positive charge will result in an increase in the activity, whereas the red contour defines a region of space where increasing the electron density is favorable. An important feature of the CoMFA model is that regions favorable to positive charges dominate the electrostatic contour map. A large blue isopleth near the 3-position of the phenyl ring represents an area, where a positive charge is favored. A fluoro or trifluoromethyl group bearing negative charges on the "F" atom diminish (**1**, **10**, **19**, **43**, and **51**) or decrease (**27–31**) the activity. As indicated in **Figure 3B**, the key catalytic negative residues of Glu636 are rather near this region, favoring a strong electrostatic interaction with the positively charged substitute group of the inhibitor. Several blue regions above the same side of the oxygen atom of the carbonyl and the oxygen atom of phosphoryl represent the area where the positively charged sodium ions could move freely. The presence of a very large blue region around the thienyl ring accounts for the decrease of activities of compounds (**35–41**), in which electronegative substituents, chloro (**35–38**), methoxy (**39**), fluoro (**40**), and nitro (**41**) groups, locate in the blue region. Electronegative groups (fluoro or chloro) at the 4-position of the phenyl ring are essential for high activities, represented by the red favorable isopleths near this area. This prediction is in agreement with the appearance of a positively charged residue of His640 at the corresponding position of the PDHc E1. As shown in **Figure 4B**, the red regions at the 2-position and 4-position of phenyl indicate that any electronegative group at these positions would enhance the activity. The blue region at the 3-position indicates that substitution of electropositive group at this position would increase the activity; however, simultaneously, the bulky substitution at the 3-position is disfavored for enhancing the activity, while the bulky substitution at the 2-position is favorable, which explains why compounds **16**, **24**, and **56** with 2-methyl have better herbicidal activity even than compounds **17**, **25**, and **57** with 3-methyl. So, the 2- and 4-positions are the most essential sites for substitution, which can enhance the herbicidal activity greatly, and compounds even with the disfavored electropositive methyl group at the 2-position still have a higher activity, which suggested that the contribution of a steric effect of the 2-position substituent for enhancing herbicidal activity was more than that of the electronic effect.

White and magenta contours of the currently reported CoMSIA model in **Figure 4C** indicate the areas where hydrophilic and hydrophobic properties were preferred, respectively, and will be useful in selecting specific areas of the molecules to be utilized for adjusting the lipophilicity and hydrophilicity to improve herbicidal activity. As shown in **Figure 4C**, the yellow area is near the 4-position of the phenyl ring just in the space where the green region appears in the steric contour of CoMFA, and it could be reasonably assumed that there is a hydrophobic cavity in the receptor, producing hydrophobic interactions with the ligands. This can be seen from the activities of compounds **3**, **13**, and **21** that possess hydrophobic groups at the 4-position, which harbors the hydrophobic residues

Tyr599, Thr525, and the counterpart of TDP887. A very distinct hydrophilic site is near the 3-position of the phenyl ring, where lower active compounds contain a methyl (8, 17, 25, 49, and 57) group as a substituent. While the activities of compounds with hydrophilic and electronegative substituents such as fluoro (1, 10, 19, 43, and 51) and trifluoromethyl (27–31) are still lower than those of compounds 8, 17, 25, 49, and 57, which could be reasonably assumed that the favorable 3-position groups should be not only hydrophilic but also electropositive and the efficacy of electropositive substituents were more important for enhancing activity than that of the hydrophilic substituents.

Validation of the 3D-QSAR Models. Eleven compounds that were not included in the training set were selected as a test data set to validate the QSAR models. All of the test compounds are well-predicted. The mean and standard deviation of prediction errors are 0.28 and 0.005 for the CoMFA model and only 0.33 and 0.011 for the CoMSIA model. The predictive r_{pred}^2 , which is analogous to the cross-validated correlation coefficient q^2 , is 0.883 for the CoMFA and 0.908 for the CoMSIA, suggesting a high reliability for these models.

The consistency between the CoMFA/CoMSIA field distributions and the 3D topology of the protein structure indicate the robustness of the 3D-QSAR models. Overall, the degree of predictivity of the CoMSIA model appeared to be similar to that of the CoMFA model, such that a combined use of both the CoMFA and the CoMSIA models may be more suitable for prediction of the activities of the novel designed compounds. On the basis of the molecular docking and 3D-QSAR studies on 1-(substituted phenoxyacetoxy)alkylphosphonates, some novel compounds have been designed and synthesized according to the above model, and the preliminary assay in a greenhouse showed that they exhibited higher herbicidal activity than that of compound 12; their inhibitions on PDHc will be further examined. To evaluate the commercial potential as an herbicide, the herbicidal activity of the active compounds will be further evaluated in the field and their acute toxicity should be first examined. We hope that some active compounds, which can be used as herbicides, will be found by an attempt to design an inhibitor of PDHc E1.

Although some expected results based on the typical 3D-QSAR have been obtained, multidimensional QSAR representing a subtle extension of 3D-QSAR (36), which allows for multiple conformation, orientation, and protonation state representation of ligand molecules and simulates the receptor-to-ligand adaptation, not only would appear to yield 3D-QSAR models at least as good as can be generated using other methods but also would provide added value information not realized by other methods (36–38). Furthermore, “variable resolution invariants” is a new approach to QSARs that makes use of 3D features of molecules at different levels of spatial resolution as well as levels of resolution in atomic properties (39). These descriptors are independent of any numbering of the atoms of a molecule. They are also independent of rigid translation and rotation of a given conformer, which avoids problems with aligning different molecules of docking them with a receptor site model (39). It is necessary for us to do a new approach to QSARs as further direction of our research.

LITERATURE CITED

- Gutowski, J. A.; Lienhard, G. E. Transition state analogs for thiamin pyrophosphate-dependent. *J. Biol. Chem.* **1976**, *251*, 2863–2866.
- Nemeria, N.; Yan, Y.; Zhang, Z.; Brown, A. M.; Arjunan, P.; Fruey, W.; Guest, J. R.; Jordan, F. Inhibition of the *Escherichia coli* pyruvate dehydrogenase complex E1 subunit and its tyrosine 177 variants by thiamin 2-thiazolone and thiamin 2-thiothiazolone diphosphates. *J. Biol. Chem.* **2001**, *276*, 45969–45978.
- Krampitz, L. O. Catalytic functions of thiamine diphosphate. *Annu. Rev. Biochem.* **1969**, *38*, 213–240.
- Jordan, F.; Nemeria, N.; Guo, F. S.; Baburina, I.; Gao, Y. H.; Kahyaoglu, A.; Li, H. J.; Wang, J.; Yi, J. Z.; Guest, J. R.; Furey, W. Regulation of thiamin diphosphate-dependent 2-oxo acid decarboxylases by substrate and thiamin diphosphate. Mg (II)—Evidence for tertiary and quaternary interactions. *Biochem. Biophys. Acta* **1998**, *1385*, 287–306.
- Dobritzsch, D.; König, S.; Schneider, G.; Lu, G. High resolution crystal structure of pyruvate decarboxylase from *Zymomonas mobilis*. *J. Biol. Chem.* **1998**, *273*, 20196–20204.
- Alvarez, F. J.; Ermer, J.; Hübner, G.; Schellenberger, A.; Schowen, R. L. Catalytic power of pyruvate decarboxylase. Rate-limiting events and microscopic rate constants from primary carbon and secondary hydrogen isotope effects. *J. Am. Chem. Soc.* **1991**, *113*, 8402–8409.
- Kern, D.; Kern, G.; Neef, H.; Tittmann, K.; Killenberg-Jabs, M.; Schneider, C. W.; Hübner, G. How thiamin diphosphate is activated in enzymes. *Science* **1997**, *275*, 67–70.
- Baillie, A. C.; Wright, K.; Wright, B. J.; Earnshaw, C. G. Inhibitors of pyruvate dehydrogenase as herbicides. *Pestic. Biochem. Physiol.* **1988**, *30*, 103–112.
- Kluger, R.; Pike, D. C. Active site generated analogues of reactive intermediates in enzymic reactions. Potent inhibition of pyruvate dehydrogenase by a phosphonate analogue of pyruvate. *J. Am. Chem. Soc.* **1977**, *99*, 4504–4506.
- Kluger, R.; Gish, G.; Kauffman, G. Interaction of thiamin diphosphate and thiamin thiazolone diphosphate with wheat germ pyruvate decarboxylase. *J. Biol. Chem.* **1984**, *259*, 8960–8965.
- He, H. W.; Wang, T.; Yuan, J. L. Synthesis and herbicidal activities of methyl-1(2,4-dichlorophenoxyacetoxy)alkylphosphonate monosalts. *J. Organomet. Chem.* **2005**, *690*, 2608–2613.
- Wang, T.; He, H. W. An efficient synthesis of α -(2,4-dichlorophenoxyacetoxy)aryl methyl phosphonate monosodium salts. *Synth. Commun.* **2004**, *34*, 1415–1423.
- Wang, T.; He, H. W. Simple and improved preparation of α -oxophosphonate monolithium salts. *Phosphorus Sulfur* **2004**, *179*, 2081–2089.
- Chen, T.; Shen, P.; Li, Y. J.; He, H. W. Synthesis and herbicidal activity of *O,O*-dialkyl phenoxyacetoxyalkylphosphonates containing fluorine. *J. Fluorine Chem.* **2006**, *127*, 291–295.
- He, H. W.; Wang, T.; Li, Y. J.; Shen, P.; Chen, T.; Liao, G. H.; Mo, W. Y. CN 1685825A, 2005.
- He, H. W.; Liu, Z. J. Progresses in research of α -oxophosphonic acid derivatives with herbicidal activity. *Chin. J. Org. Chem.* **2001**, *21*, 878–883.
- Wang, T.; He, H. W.; Yuan, J. L. PDH: A new reacting target for herbicide. *Chin. J. Appl. Chem.* **2003**, *20*, 613–617.
- Tan, H. L.; Yuan, J. L.; He, H. W.; Wang, T. Effects of methylphosphonate monosodium on pyruvate dehydrogenase. *Chin. J. Chem. Eng.* **2005**, *6*, 4–5.
- Arjunan, P.; Nemeria, N.; Brunskill, A.; Chandrasekhar, K.; Sax, M.; Yan, Y.; Jordan, F.; Guest, J. R.; Furey, W. Structure of the pyruvate dehydrogenase multienzyme complex E1 component from *Escherichia coli* at 1.85 Å resolution. *Biochemistry* **2002**, *41*, 5213–5221.
- Arjunan, P.; Chandrasekhar, K.; Sax, M.; Brunskill, A.; Nemeria, N.; Jordan, F.; Furey, W. Structural determinants of enzyme binding affinity: The E1 component of pyruvate dehydrogenase from *Escherichia coli* in complex with the inhibitor thiamin thiazolone diphosphate. *Biochemistry* **2004**, *43*, 2405–2411.
- Chakraborty, K.; Devakumar, C. Quantitative structure-activity relationship analysis as a tool to evaluate the mode of action of chemical hybridizing agents for wheat (*Triticum aestivum* L.). *J. Agri. Food. Chem.* **2005**, *53*, 3468.

- (22) Cramer, R. D.; Patterson, D. E., III; Bunce, J. D. Comparative molecular field analysis (CoMFA). 1. Effect of shape on binding of steroids to carrier proteins. *J. Am. Chem. Soc.* **1988**, *110*, 5959–5967.
- (23) Klebe, G.; Abraham, U.; Mietzner, T. Molecular similarity indices in a comparative analysis (CoMSIA) of drug molecules to correlate and predict their biological activity. *J. Med. Chem.* **1994**, *37*, 4130–4146.
- (24) Yang, H. Z.; Zhang, Y. J.; Wang, L. X.; Tan, H. F.; Cheng, M. R.; Xing, X. D.; Chen, R. Y.; Fujita, T. Quantitative structure-activity study of herbicidal *O*-aryl *O*-ethyl *N*-isopropylphosphoramidothioates. *Pestic. Biochem. Physiol.* **1986**, *26*, 275–283.
- (25) Yang, G. F.; Liu, H. Y.; Yang, H. Z. QSAR and 3D-QSAR analysis of structurally diverse ALS inhibitors: Sulfonylureas and triazolopyrimidine-2-sulfonamides. *Pestic. Sci.* **1999**, *55*, 1143–1150.
- (26) Morris, G. M.; Goodsell, D. S.; Huey, R.; Hart, W. E.; Halliday, R. S.; Belew, R. K.; Olson, A. J. *Autodock*, Version 3.0.5; Department of Molecular Biology, Molecular Graphics Laboratory, The Scripps Research Institute: LaJolla, CA, 2001.
- (27) SYBYL, version 7.0; Tripos Inc.: St. Louis, 2004.
- (28) Clark, M. C.; Cramer, R. D.; Van Opdenbosch, N., III. Validation of the general purpose tripos 5.2 force field. *J. Comput. Chem.* **1989**, *10*, 982–1012.
- (29) Powell, M. J. D. Restart procedures for the conjugate gradient method. *Math. Program* **1977**, *12*, 241–254.
- (30) Morris, G. M.; Goodsell, D. S.; Halliday, R. S.; Huey, R.; Hart, W. E.; Belew, R. K.; Olson, A. J. Automated docking using a Lamarckian genetic algorithm and an empirical binding free energy function. *J. Comput. Chem.* **1998**, *19*, 1639–1662.
- (31) Wold, S.; Rhue, A.; Wold, H.; Dunn, W. J. I. The covariance problem in linear regression. The partial least squares (PLS) approach to generalized inverses. *SIAM J. Sci. Stat. Comput.* **1984**, *5*, 735–743.
- (32) Wold, S.; Albano, C.; Dunn, W. J., III; Edlund, U.; Esbensen, K.; Geladi, P.; Hellberg, S.; Johanson, E.; Lindberg, W.; Sjostrom, M. Multivariate data analysis in chemistry. *NATO ASI Ser. Ser. C* **1984**, *138*, 17–95.
- (33) Clark, M.; Cramer, R. D., III. The probability of chance correlation using partial least squares (PLS). *Quant. Struct.-Act. Relat.* **1993**, *12*, 137–145.
- (34) Bush, B. L.; Nachbar, R. B. Sample-distance partial least-squares PLS optimized for many variables, with application to CoMFA. *J. Comput.-Aided Mol. Des.* **1993**, *7*, 587–619.
- (35) Boulamwini, J. K.; Assefa, H. CoMFA and CoMSIA 3D QSAR and docking studies on conformationally-restrained cinnamoyl HIV-1 integrase inhibitors: exploration of a binding mode at the active site. *J. Med. Chem.* **2002**, *45*, 841–852.
- (36) Lill, M. A.; Dobler, M.; Vedani, A. Multi-dimensional QSAR in drug discovery: Probing ligand alignment and induced fit-application to GPCRs and nuclear receptors. *Curr. Comput.-Aided Drug Des.* **2005**, *1*, 307–324.
- (37) Hopfinger, A. J.; Wang, S.; Tokarski, J.; Jin, B.; Albuquerque, M.; Madhav, P. J.; Duraiswami, C. Construction of 3D-QSAR models using the 4D-QSAR analysis formalism. *J. Am. Chem. Soc.* **1997**, *119*, 10509–10524.
- (38) Vedani, A.; Dobler, M. 5D-QSAR: The key for simulating induced fit? *J. Med. Chem.* **2002**, *45*, 2139–2149.
- (39) Crippen, G. M. VRI: 3D QSAR at variable resolution. *J. Comput. Chem.* **1999**, *20*, 1577–1585.

Received for review September 22, 2006. Revised manuscript received December 20, 2006. Accepted December 27, 2006. We acknowledge financial support of this work by National Key Basic Research Development Program of China (“973” Projects 2003CB114406 and 2004CCA00100), National Natural Science Foundation of China (20072008 and 20372023), Natural Science Foundation of Hubei Province (2005ABB012 for Distinguished Young Scholar and 2004ABC002 for Innovation Group), Science and Technology Research Project of Ministry of Education (106116), CNGI-04-15-7A, and China National Technology Platform.

JF062730H